

Spectral transport of nonequilibrium 29-cm⁻¹ phonons in ruby studied by fluorescence line narrowing

M. J. van Dort, J. I. Dijkhuis, and H. W. de Wijn

Faculty of Physics and Astronomy, University of Utrecht, P.O. Box 80 000, 3508 TA Utrecht, The Netherlands

(Received 31 July 1989)

A new method, based on fluorescence line narrowing, is presented for the detection of near-resonant trapped phonons with an extremely high spectral resolution. The method is applied to 29-cm⁻¹ phonons resonant with the inhomogeneous $\bar{E}(^2E)-2\bar{A}(^2E)$ transition of Cr³⁺ in ruby (Al₂O₃:Cr³⁺) following injection of a flat spectrum of nonequilibrium phonons into the crystal. Spectral transport within the trapped phonon packet is observed directly from the shape of the phonon spectrum around $\bar{E}(^2E)-2\bar{A}(^2E)$ as it develops with time. An account is first given in terms of phenomenological rate equations with inclusion of the variations of the spin-phonon coupling through the transition as well as spectral transport. The dynamics of the 29-cm⁻¹ phonons in frequency and space is understood more quantitatively from Monte Carlo simulations following the life history of the phonons. Generally good agreement is found with an earlier model based on weakly exchange-coupled Cr³⁺ pairs, in which the phonon frequency, and as a result the mean free path, are modified by one-site resonant Raman processes, and diffusive motion is terminated by ballistic escape out of the hot zone.

I. INTRODUCTION

The principal objective of this paper is to show that the technique of fluorescence line narrowing (FLN) allows us to examine the dynamics of nonequilibrium phonons with high spectral resolution. More specifically, FLN is applied to the problem of spectral transport of trapped high-frequency phonons by resonant-scattering centers, and subsequently an analysis is made in terms of a microscopic model based on pair interactions. Much of the work to date on the dynamics of high-frequency phonons has been carried out for ruby (Al₂O₃:Cr³⁺), in which 29-cm⁻¹ phonons near resonance with the $\bar{E}(^2E)-2\bar{A}(^2E)$ transition interact strongly with Cr³⁺ maintained in the $\bar{E}(^2E)$ state. In the event metastable Cr³⁺ are made sufficiently dense, multiple absorption and emission of the phonons establishes a dynamical equilibrium of phonons and spins (phonon bottleneck), which is reflected in an elongation of the time for return from $2\bar{A}(^2E)$ to $\bar{E}(^2E)$. The dynamics of 29-cm⁻¹ phonons trapped in the optically excited zone can thus be studied by monitoring the phonon-induced R_2 luminescence emanating from $2\bar{A}(^2E)$.¹ It is found that the effective relaxation time T_{eff} of the $2\bar{A}(^2E)$ occupation not only increases with the excited-state concentration N^* , but further with the typical dimension L of the excited zone.²⁻⁴ This, of course, points to phonon loss predominantly by escape out of the active zone, consistent with earlier experiments,⁵ which indicated that the lifetime of the 29-cm⁻¹ phonons against anharmonic decay is at least 1 μ s. In fact, at a low concentration of excited ions ($N^*L \lesssim 10^{15}$ cm⁻²), the dynamics of the trapped phonons is determined by spatial diffusion.² At higher N^* , spatial diffusion is too slow a process, and mechanisms involving spectral transfer to such a distance from resonance that the mean free path

overcomes L , dominate the phonon dynamics.^{3,4,6}

Direct evidence for spectral transport is, however, limited. In an early cw experiment,⁷ the spectral width of the nonequilibrium phonon spike resonant between $\bar{E}(^2E)$ and $2\bar{A}(^2E)$ was derived from the magnetic field dependence of the phonon bottleneck. Spectral diffusion was apparent from an increase of the spectral width with N^* . It has been realized that exchange-coupled Cr³⁺ pairs play a major role in spectral transport. Strong exchange-coupled pairs were demonstrated to mediate in efficient spectral transport over large distances at high N^* from a growth of the "hot"- N_2 -pair luminescence.⁶ Compelling spectroscopic evidence for the involvement of more weakly coupled pairs in the relaxation of 29-cm⁻¹ phonon was derived from the temporal development of the R_1 spectra of these pairs, situated in the wings of the single-ion R_1 line, following injection of nonequilibrium phonons by means of heat pulses.⁸ The involvement of $2\bar{A}(^2E)$ was established from a notable luminescence near R_2 . Another recent experiment was designed specifically for the observation of spectral transport over fixed larger distances.⁹ A far-infrared laser was used to generate monochromatic phonons in a crystal doped with Cr²⁺, Cr³⁺, and V⁴⁺ ions. The V⁴⁺ ions acted both as phonon generators at either 25.8 or 27.8 cm⁻¹ and as resonant scattering centers, and Cr²⁺ were assumed to be the major inelastic scatterers. The $\bar{E}(^2E) \rightarrow 2\bar{A}(^2E)$ resonance of the Cr³⁺ ions was used for detection of phonons displaced to 29.1 cm⁻¹. While these experiments confirm the presence of spectral transport, they are not suited for the spectral regime near the borderline between trapped and ballistic phonons, located at about 1 GHz from resonance for a typical $N^*L \sim 10^{15}$ cm⁻², nor for the observation of the trapped phonon packet itself. The new method of phonon spectroscopy based on FLN, developed below, employs high-resolution

optical techniques to detect the trapped phonons both as a function of time and spectral frequency, and permits the examination of the very regime relevant to the phonon bottleneck. The method to derive the phonon spectra from the measured FLN spectra is described in detail in Sec. II.

Two principal mechanisms shifting the frequency of the trapped 29-cm^{-1} phonons have been considered. The mechanisms have in common that the shifts are provided by weakly exchange-coupled Cr^{3+} pairs made up of a Cr^{3+} in the $\bar{E}(^2E)$ excited state and a Cr^{3+} in the 4A_2 ground state. One of these is resonant phonon-assisted energy transfer,¹⁰ in which the optical excitation is transferred to the other member of the pair by off-diagonal exchange, and the balance in excitation energy δE is carried away or supplied by a 29-cm^{-1} phonon.³ For the mechanism to be effective, microscopic broadening, i.e., mismatch of the optical transitions of the Cr^{3+} constituting the pair, must be present. For reasonable values of the exchange and microscopic broadening of R_1 , the mechanism appears to overestimate the phonon loss by 2 orders of magnitude, indicative of the absence of appreciable energy mismatch for the relevant pairs (Cr^{3+} separation $\lesssim 10 \text{ \AA}$). Indeed, despite extensive and explicit searches,¹¹⁻¹³ energy transfer has not been found to take place but at millisecond time scales, even in more concentrated ruby and at higher temperatures. Also, the dependences of the transfer rate on temperature and energy mismatch were found to be inconsistent with resonant phonon-assisted energy transfer.¹⁴

The other mechanism is based on one-site resonant Raman (Orbach) transitions of Cr^{3+} weakly coupled to a nearby Cr^{3+} in the 4A_2 ground state by diagonal exchange.⁴ It involves the absorption of a resonant phonon from $\bar{E}(^2E)$ to $2\bar{A}(^2E)$ in a spin-nonflip transition, followed by a spin-flip transition back to the $\bar{E}(^2E)$ level, shifting the phonon energy by an amount equal to the exchange splitting. Energy displacements such that the scattered phonon is able to reach the unpumped region ballistically is taken to constitute a "wipeout." Within the uncertainties of the parameters, the mechanism has previously been found to account for the 29-cm^{-1} phonon relaxation as a function of N^* , the size of the excited zone, and a magnetic field.^{4,15}

Below (Sec. IV), we will first consider a number of general features of the shape of the trapped phonon packet obtained with FLN. Subsequently, we parametrize the temporal development of the spectra in terms of a tractable phenomenological formulation based on rate equations containing phonon loss and spectral transfer. Next (Sec. V), a quantitative calculation of spectral phonon loss is performed in terms of the microscopic model of one-site resonant Raman processes modifying the phonon frequency until escape is achieved. Since the problem defies analytical treatment, reliance is made on Monte Carlo techniques, with due account for the shape of the transition and with proper distinction between the rates of the various spin-nonflip and spin-flip $\bar{E}(^2E)$ - $2\bar{A}(^2E)$ transitions. A subsequent comparison with the experimental phonon spectra provides further support for the one-site resonant Raman mechanism of spectral shifting.

II. METHOD

The experimental technique developed in this paper for time-dependent spectroscopy of high-frequency phonons is based on FLN. The technique of FLN is a method in laser spectroscopy in which the inhomogeneous broadening is overcome by selective excitation of a homogeneous subset of the optical centers. It is, in this regard, related to hole burning of the ground state by saturation. In solids, FLN was first accomplished by Szabo¹⁶ for the case of ruby. Fields that since then have particularly benefitted from the technique are energy transfer and optical dephasing.¹⁷ Here, FLN is made suitable for the observation of the spectrum of nonequilibrium high-frequency phonons as it evolves with time. A three-level scheme is used (Fig. 1). A homogeneous subset of the optical centers is first excited by narrow-band optical excitation to a metastable state. The centers thus prepared subsequently act as luminescent phonon detectors via phonon-assisted excitation to a third nearby level and the subsequent luminescent return to the ground state. The phonon spectrum, then, finds itself reflected in the line shape of the emanating luminescence.

In the present experiments, phonon-induced FLN is applied to 29-cm^{-1} phonons at or near resonance with the $\bar{E}(^2E)$ - $2\bar{A}(^2E)$ transition of excited Cr^{3+} in dilute ruby. A homogeneous packet of Cr^{3+} in $\bar{E}(^2E)$ is maintained by continuous excitation out of the 4A_2 ground state. The phonons are injected by an external pulsed heater, providing an initially flat phonon spectrum. The spectrum, however, modifies with time by virtue of scattering off excited Cr^{3+} . Thermal phonons are removed by cooling down to approximately 1.5 K. In ruby, even under weak optical pumping severe trapping of phonons is established, i.e., the time τ_{res} before a phonon takes part in a transition $\bar{E}(^2E) \rightarrow 2\bar{A}(^2E)$ is many times shorter ($\sim 0.3 \text{ ns}$ at $N^* \sim 10^{17} \text{ cm}^{-3}$) than the lifetime against removal out of the trapped zone ($\gtrsim 30 \text{ ns}$). Upon ignoring for the moment the finite homogeneous width of

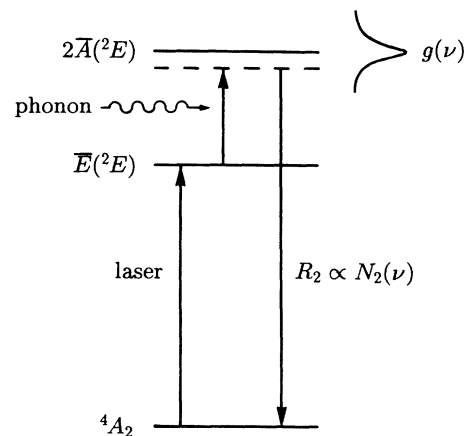


FIG. 1. Principle of frequency-selective phonon detection. The $\bar{E}(^2E)$ level is homogeneously populated. Incoming phonons raise Cr^{3+} to $2\bar{A}(^2E)$, resulting in an R_2 luminescence of a shape reflecting the phonon spectrum.

the $\bar{E}(^2E)$ state, the $2\bar{A}(^2E)$ population then is dictated by the bottlenecking condition

$$N_2(\nu, t) = N^* g(\nu) p(\nu, t), \quad (1)$$

in which $p(\nu, t)$ is the time-dependent occupation number of the phonon modes with frequency ν , and $g(\nu)$ is the normalized shape of the $\bar{E}(^2E)$ - $2\bar{A}(^2E)$ transition. Bottlenecking implies that dynamical equilibrium is established between the phonons and the spin system. So any modification of $p(\nu, t)$ goes associated with a similar modification of $N_2(\nu, t)$, and it is the combined spin-phonon system that reacts to an outside disturbance, such as an externally supplied phonon spectrum. Dynamical equilibrium is indeed attained at much shorter time scales. As is straightforwardly derived, its time constant is made up of $\tau_{\text{res}} = \rho T_d / N^* g(\nu)$ in parallel with T_d , where T_d is the spontaneous decay time of $2\bar{A}(^2E)$ to $\bar{E}(^2E)$ against emission of a phonon ($T_d \sim 1$ ns), and ρ is the density of phonon states. It is further noted that the absorption of a phonon by Cr^{3+} entails energy conservation, but not necessarily conservation of momentum.

Following absorption of phonons, Cr^{3+} in $2\bar{A}(^2E)$ has a small, but finite, probability of returning to the 4A_2 ground state. According to Eq. (1), the associated R_2 luminescence contains, in its shape, the phonon spectrum we wish to measure. With allowance for the finite width of the optical transition [full width at half maximum (FWHM) 65 ± 10 MHz (Ref. 18)], the R_2 intensity, in fact, scales with the convolution

$$R_2(\nu, t) = N_2(\nu, t) * \bar{R}_1(\nu) \\ = \int N_2(\nu - \nu', t) \bar{R}_1(\nu') d\nu', \quad (2)$$

in which $\bar{R}_1(\nu)$ is the normalized line shape of the R_1 optical transition under high-resolution excitation. The line shape $\bar{R}_1(\nu)$ is mainly due to hyperfine interactions, but may also account for residual inhomogeneous broadening and, for that matter, a finite width of the laser frequency.

In summary, the phonon spectrum is obtained by observing $R_2(\nu, t)$ under high resolution, correcting $R_2(\nu, t)$ for $\bar{R}_1(\nu)$ by deconvolution, and dividing the result by $g(\nu)$. The technique is, of course, only useful in a range covering a few times the linewidth of the phonon transition. This is not a very serious limitation, however, since this is precisely the part of the phonon spectrum of relevance to processes involving trapping by the centers. It is also noted that the existence of a bottleneck, although enhancing $N_2(\nu, t)$, is not essential. Besides, the phonon transition may, in many cases, be tuned to some extent. The line shape $g(\nu)$ has been directly found from far-infrared absorption spectroscopy,¹⁹ or may be measured with FLN.²⁰ For the scheme to work best, the energy distribution of the $\bar{E}(^2E)$ metastable population further should remain sufficiently narrow in relation to $g(\nu)$. In other terms, no appreciable off-resonant energy transfer from one packet to another should occur within the radiative lifetime τ_R (≈ 4 ms). Finally, to ensure one-to-one correspondence between $N_2(\nu, t)$ and $p(\nu, t)$, the predominant dephasing of $2\bar{A}(^2E)$ must be by one-phonon emission. In ruby these conditions are fulfilled at low temperatures.

III. EXPERIMENTAL DETAILS

A cw ring dye laser (Spectra physics model 380D operating with Exciton LD 688 dye and pumped with a 10-W Ar-ion laser), maintains the $\bar{E}(^2E)$ population of Cr^{3+} by direct optical excitation out of the 4A_2 ground state at the wavelength of the R_1 transition (693.4 nm at 1.5 K). More precisely, the laser wavelength is set at one of the peaks of the inhomogeneous axial-field split R_1 . (It has been verified that the phonon dynamics is independent of the choice between the two peaks, except through N^* .) The dye laser is actively stabilized and has a bandwidth of order 1 MHz or better. The power of the exciting beam is typically 20–50 mW. To ensure single-mode operation and the absence of long-term drift of the dye laser, its frequency is continually monitored with a spectrum analyzer with a 2-GHz free spectral range. The excited zone has the shape of a cylinder with a diameter ranging from 30 μm to several hundreds of μm , as defined by the laser beam, focused inside the crystal. The detected volume is further limited by the receiving optics. The position of the zone is chosen close to the surface to minimize reabsorption of the luminescence.

The crystal, either a Czochralsky-grown 700-at.-ppm ruby of dimensions $4 \times 4 \times 4$ mm³ or a Verneuil-grown 2500-at.-ppm ruby of $3 \times 3 \times 6$ mm³ in size, is held at 1.5 K by immersion in pumped liquid helium. Nonequilibrium phonons are injected by a constantan heater, as first accomplished by von Gutfeld and Nethercot.²¹ The heater, deposited onto the specimen by evaporation, has a thickness of 40 nm and an area of 1×1 mm² [resistance (10–20) Ω]. The heater is driven with a pulse generator during 100-ns periods at 3- μs intervals. The peak power dissipated is 10 W. The phonon spectrum injected, which is known to be adequately described by a Planckian distribution corresponding to a temperature of order 10 K,²² may be considered essentially flat around the $\bar{E}(^2E)$ - $2\bar{A}(^2E)$ transition. The Bose-Einstein occupation numbers of the 29-cm⁻¹ phonons typically are of order 3×10^{-2} , as determined from the ratio of R_2 and R_1 intensities. This corresponds to an effective temperature of 11 K. The zone of detection, a cylinder with radius R located adjacent to the heater, is defined by the extent of the excited zone, and further by the receiving optics and the apertures of the pinholes used. It has a length of 100 μm and a diameter of, at maximum, 200 μm , corresponding to ballistic flight times through the detection zone of, at most, 20 ns.

The R_2 light, collected at right angles to the incident laser beam, is analyzed with a temperature-stabilized single-pass Fabry-Perot interferometer. The free spectral range is set at 3.5 GHz for the 700-at.-ppm sample, and at 7.0 GHz for the 2500-at.-ppm sample. The finesse is, in all cases, larger than 30, resulting in instrumental resolutions of about 100 and 200 MHz, respectively. A 0.85-m double monochromator, tuned to the R_2 wavelength, is inserted into the optical path to suppress the R_1 and pair luminescences. Standard photon-counting equipment is used. Time resolution is provided by time-to-amplitude conversion techniques. A computer, equipped with a multichannel-analyzer card, provides both data ac-

quisition and control of the mirror spacing of the interferometer.

The observed R_2 spectra need, of course, to be deconvoluted for the instrumental profile of the optical detection system to obtain the intrinsic R_2 intensity. That is,

$$R_2^{(\text{obs})}(\nu, t) = R_2(\nu, t) * I(\nu), \quad (3)$$

where $I(\nu)$ represents the instrumental profile, which is primarily determined by the alignment of the interferometer mirrors. The precaution has been taken to register $I(\nu)$ after each measurement by passing part of the incoming laser light directly through the interferometer with the monochromator set at the laser frequency. These profiles have subsequently been parametrized, and entered into the deconvolution procedure.

IV. RESULTS

An example of the measured R_2 intensity as a function of frequency and time is presented in Fig. 2. Data sets such as in Fig. 2 are built up by repetitive stepwise scanning through the R_2 spectrum over a distance covering the free spectral range of the interferometer. Typically 30 passes through the spectrum were recorded in a matrix of 128 channels in frequency of 256 channels in time. The passes were of 1-min duration, so that at each of the corresponding 128 interferometer settings about 5×10^6 time evolutions of the R_2 intensity were accumulated. In order to derive the phonon spectrum $p(\nu, t)$ at a given time from these data, we apply the procedures outlined above, i.e., we (i) deconvolute the observed R_2 spectrum for the instrumental profile to obtain $R_2(\nu, t)$ [cf. Eq. (3)], (ii) deconvolute $R_2(\nu, t)$ for the homogeneous width of the R_1 transition [cf. Eq. (2)], and (iii) divide the resultant

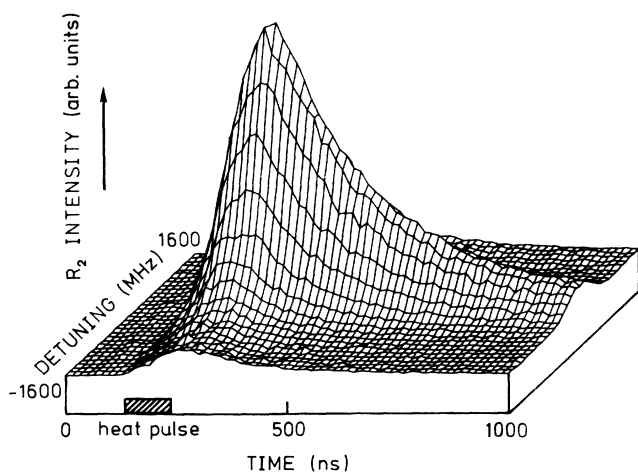


FIG. 2. A typical example of the heat pulse induced R_2 luminescence vs time and frequency for 700-at.-ppm ruby at $N^* \approx 1.5 \times 10^{17} \text{ cm}^{-3}$ and $2R \approx 200 \mu\text{m}$. The mesh shows only 1 in 16 data points. Phonons are injected along the c axis. The scattering plane is transverse to the c axis, with the incoming light polarized in the plane to suppress R_2 emission to the other component of the 4A_2 state.

$N_2(\nu, t)$ by the line shape of the phonon transition $g(\nu)$ [cf. Eq. (1)]. To facilitate the computations, the first two steps were, in practice, carried out by double convoluting an analytical form of $N_2(\nu, t)$ with $I(\nu)$ and $\bar{R}_1(\nu)$, and adjusting the parameters occurring in $N_2(\nu, t)$ such as to achieve coincidence of the result with the observed R_2 spectrum. Here, a representation of $N_2(\nu, t)$ by a Lorentzian to a power of order unity generally appeared adequate. The homogeneous FWHM of the R_1 transition is known from previous FLN work to amount to $\Delta\nu_{\text{hom}, R} = 65 \pm 10 \text{ MHz}$ in zero magnetic field.¹⁸ This is only marginally smaller than the instrumental width of the interferometer, but substantially smaller than the width of the observed R_2 line, which typically amounts to 450 and 1150 MHz for the 700-at.-ppm and 2500-at.-ppm cases, respectively.

In particular, in the wings of $g(\nu)$, the division of $N_2(\nu, t)$ by the line shape of the phonon transition $g(\nu)$, necessary to obtain the phonon spectra, may introduce substantial errors.²³ Considerable care has therefore been taken to determine $g(\nu)$, and to arrive at a faithful analytical representation extending over several times its width. In fact, $g(\nu)$ has been independently measured with FLN; this method has the advantage that it may be carried out *in situ*, and further allows one to discern between the homogeneous and inhomogeneous widths of the phonon transition.²⁰ This is of relevance because the inhomogeneous part depends strongly on the specific crystal, especially on the ground-state concentration and the method of growing. As it turns out, the phonon transition is accurately described by a Voigt profile over a distance of 1500 MHz to either side for the 700-at.-ppm crystal, and twice this range for the 2500-at.-ppm case. The homogeneous (Lorentzian) contribution, determined by the lifetime of the $2\bar{A}({}^2E)$ level, appears not to depend on the crystal. We find for the homogeneous FWHM $\Delta\nu_{\text{hom}} = 240 \pm 15 \text{ MHz}$.²⁰ This corresponds to $T_d = 0.66 \pm 0.04 \text{ ns}$, in agreement with a precision measurement of T_d with accumulated phonon echo.²⁴ The inhomogeneous (Gaussian) width $\Delta\nu_{\text{inh}}$ amounts to $295 \pm 15 \text{ MHz}$ for the 700-at.-ppm Czochralsky-grown crystal, and $935 \pm 35 \text{ MHz}$ for the 2500-at.-ppm Verneuil-grown crystal.

Examples of the temporal development of the phonon spectrum $p(\nu, t)$ around resonance are presented in Fig. 3 for 700-at.-ppm ruby with $N^* = 1.5 \times 10^{17} \text{ cm}^{-3}$ and in Fig. 4 for 2500-at.-ppm ruby with $N^* = 4 \times 10^{17} \text{ cm}^{-3}$. The graphs for $p(\nu, t)$ at various N^* constitute the primary result of the experiment. Note that, at a given time, the noise has been taken out as a result of adopting an analytical form for $N_2(\nu, t)$ in the deconvolution procedure. As to the accuracy of $p(\nu, t)$, we note that it is primarily governed by the statistical error in $R_2(\nu, t)$ and the uncertainties in the Voigt profile $g(\nu)$. The errors introduced by deconvoluting for $\bar{R}_1(\nu)$ is of order 1% for 700-at.-ppm and negligible for 2500-at.-ppm, while deconvoluting for the instrumental profile $I(\nu)$ introduces even smaller errors. In the case of Fig. 3, for example, the uncertainty due to the statistical error of $R_2(\nu, t)$ amounts to 2% at zero detuning and time 200 ns. While

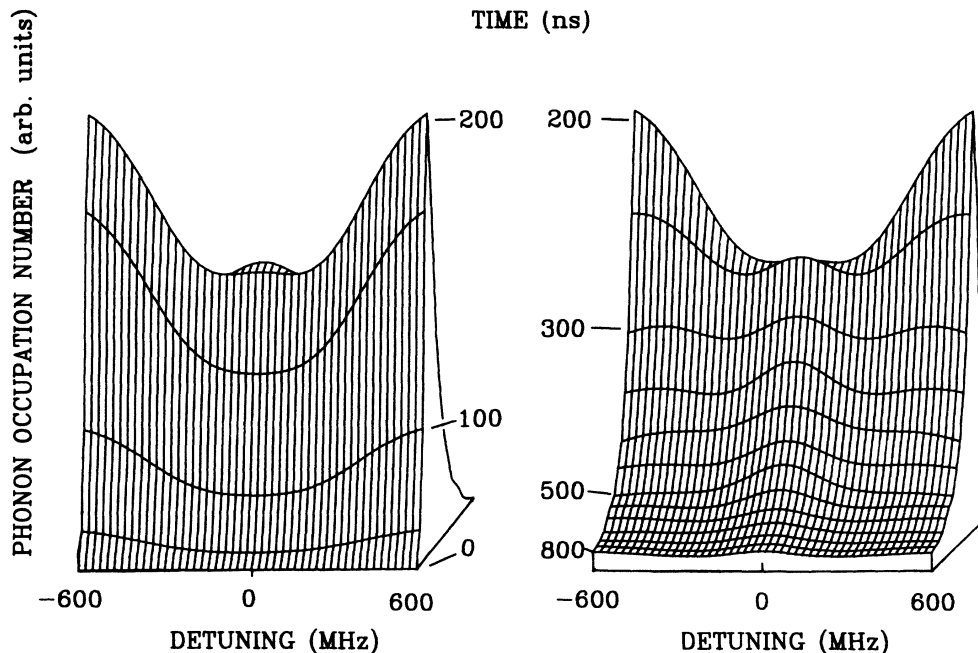


FIG. 3. Phonon spectrum vs time following a heat pulse of 100-ns duration for the 700-at.-ppm ruby at $N^* \approx 1.5 \times 10^{17} \text{ cm}^{-3}$ and $2R \approx 200 \mu\text{m}$. At resonance, $p(\nu, t)$ reaches a maximum value of about 3×10^{-2} . At any given time, experimental noise has been averaged out in the deconvolution procedure.

the error in $p(\nu, t)$ due to $R_2(\nu, t)$ and $g(\nu)$ thus totals a few percent at resonance, the shape of $p(\nu, t)$ versus ν is less well defined.²⁵ More specifically, in Fig. 3 the statistical error of $R_2(\nu, t)$ has increased to 10% at ± 600 MHz detuning. The error in $p(\nu, t)$ is further augmented with a 4% contribution due to $g(\nu)$. For the 2500-at.-ppm

case (Fig. 4) at 300 ns, the combined error runs from 2% at resonance to about 10% at a detuning of ± 1200 MHz.

We first qualitatively discuss a few noteworthy general features of $p(\nu, t)$, and then consider some aspects of the phonon dynamics in greater detail, primarily by a comparison of $p(\nu, t)$ at different N^* and Cr^{3+} ground-state

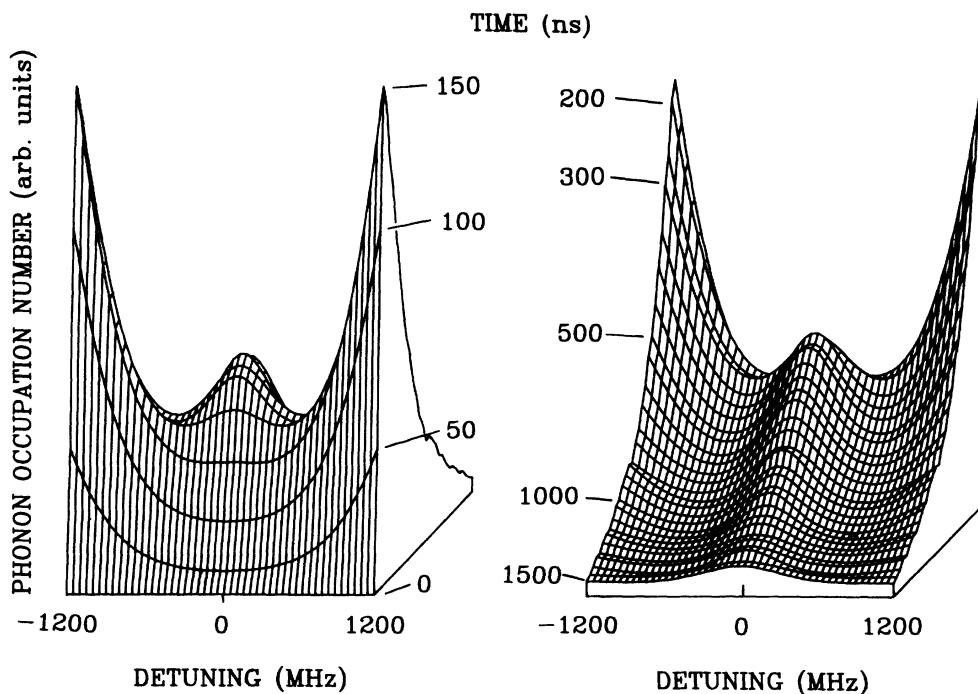


FIG. 4. Same as Fig. 3, but for 2500-at.-ppm ruby at $N^* \approx 4 \times 10^{17} \text{ cm}^{-3}$ and $2R \approx 200 \mu\text{m}$. At resonance, $p(\nu, t)$ reaches 3×10^{-2} .

concentrations. The most salient feature of Figs. 3 and 4 is that the phonon spectrum at the shorter times exhibits a pronounced depression around resonance. The physical explanation for the dip is twofold: (i) initially the spin system preferentially absorbs resonant phonons, and (ii) resonant phonons supplied by an outside source only marginally penetrate the excited zone because of strong diffusive scattering, and therefore escape detection. As to (i), we recall that under bottlenecking conditions the phonons maintain a dynamical equilibrium with the spin system, as expressed by Eq. (1), on a time scale of τ_{res} in parallel with T_d . Not too far from resonance, where the "heat capacity" of the combined system primarily resides with the spins [$N^*g(\nu) \gg \rho$], dynamical equilibrium thus is established within times shorter than 1 ns. On a much longer time scale, the combined spin-phonon system in turn strives for equilibrium with, on the one hand, the phonons supplied by the heater and, on the other hand, the phonon loss. Upon ignoring for the moment spectral transport, the time constant in fact is

$$T_{\text{eff}}(\nu) = [N^*g(\nu)/\rho + 1]\tau, \quad (4)$$

with τ the phonon lifetime. Through $g(\nu)$, the ingrowth of $N_2(\nu, t)$ thus is slowest at resonance, which results in a dip at short times. In the relevant range of frequencies, the shape of the dip is approximately given by $1/g(\nu)$, i.e., a reciprocal Voigt profile, while its depth is determined by the ratio N^*/ρ of the heat capacities of spins and phonons. In Figs. 3 and 4, such a dependence is indeed qualitatively verified for the data at short times (< 100 ns). In connection with (ii), we briefly note here that the mean free path of phonons against elastic scattering off Cr^{3+} ions amounts to

$$\Lambda(\nu) = \rho v T_d / N^* g(\nu), \quad (5)$$

where v is the phonon velocity. At resonance ($\nu = \Delta$), where $\Lambda(\Delta) \approx 2 \mu\text{m}$ for the N^* pertaining to Fig. 3, phonons therefore experience their first scattering event very near the surface of the hot zone. Because of the presence of the surface, however, a considerable fraction of these resonant phonons escape back into the unpumped region after a random walk over only a short distance. In fact, they do not succeed, as they would in the bulk, in completing σ diffusive steps covering a distance $\sigma^{1/2}\Lambda$, where the bottlenecking parameter σ expresses the number of interruptions of a phonon during its lifetime. Simple considerations show that the average number of interruptions experienced by a phonon starting at the surface is reduced by a factor of order $\sigma^{1/2}$ compared with the bulk.²⁶ The penetration depth thus is of order $\sigma^{1/4}\Lambda$, or only $9 \mu\text{m}$ at the appropriate $\sigma \sim 500$.

A second feature of Figs. 3 and 4 worth noticing is that at longer times the return of the phonon population to zero becomes faster with the distance from resonance. Evidently, this is in qualitative conformity with the drop of T_{eff} with detuning. It is important to note at this point, however, that the comparison entirely fails when made quantitative upon adopting a $T_{\text{eff}}(\nu)$ varying according to Eq. (4). More specifically, Eq. (4) overestimates the depression at short times, while the peaking up

of the trapped-phonon spectrum calculated from Eq. (4) at longer times is more pronounced than observed. Any reasonable frequency-dependent τ in lieu of a constant τ , i.e., exhibiting a maximum at $\nu = \Delta$, would only aggravate the lack of agreement. The cause obviously is that we have considered the phonon spectrum as made up of isolated packets, thereby ignoring any communication. Spectral transfer indeed tends to equalize the phonon occupations.

The question arises whether the depression in the phonon spectrum around resonance would persist in the event the external phonon feeding is maintained over longer times. This situation is of interest because the effects of the spin heat capacity, discussed above, are eliminated under stationary conditions [cf. Eq. (6) below], i.e., in the event the external phonon feeding is of a duration sufficiently long for the individual phonon packets to reach equilibrium with phonon supply and decay (T_{eff}), and for spectral redistribution among the packets to be completed. The results of FLN experiments with a heat pulse of 800-ns duration are summarized in Fig. 5 for the 700-at.-ppm case with $N^* \approx 1.5 \times 10^{17} \text{ cm}^{-3}$. The width of $N_2(\nu, t)$ is observed to stabilize towards the end of the heat pulse at a FWHM of 640 MHz. Only after the heat pulse has been switched off is the width seen to decline to the FWHM of 420 MHz belonging to the line shape $g(\nu)$, which corresponds to a return to a flat spectrum of the phonon populations. Under stationary conditions, therefore, the width of N_2 versus ν is substantially above the width of $g(\nu)$. This is indeed indicative of a depression in the phonon spectrum. As a case in point, in the inset of

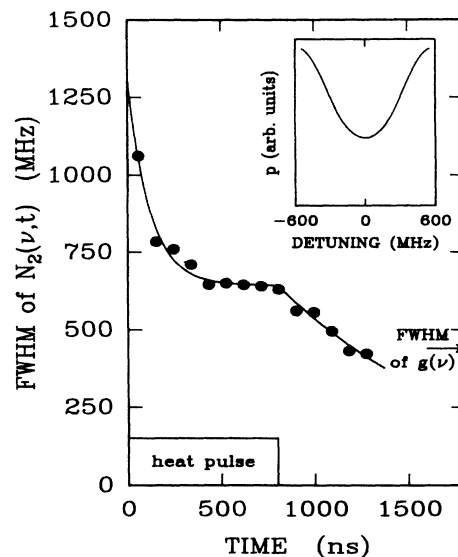


FIG. 5. Width of the R_2 luminescence vs time after deconvolution for $I(\nu)$ and $\bar{R}_1(\nu)$ in the case of a heat pulse of long duration for 700-at.-ppm ruby at $N^* = 1.5 \times 10^{17} \text{ cm}^{-3}$ and $2R \approx 200 \mu\text{m}$. The inset shows the phonon spectrum at the end of the heat pulse, i.e., under quasistationary conditions. Note that in the quasistationary regime, the width of $N_2(\nu, t)$ exceeds the width of $g(\nu)$.

Fig. 5 the phonon population derived from $N_2(\nu, t)$ versus ν at 800 ns is displayed as a function of the detuning. Self-evidently, in the stationary case a dip in the phonon spectrum only develops if there is no significant direct feeding of resonant phonons.

Quantitative conclusions with regard to spectral transport are ultimately gained from the detailed analysis below (Sec. V B). Before turning to this, however, we first demonstrate that upon closer inspection the physical significance of spectral transport is already apparent from $N_2(\nu, t)$. In Fig. 6, the width of the observed line shape $N_2(\nu, t)$ is, after deconvolution, plotted as a function of time for both the 700-at.-ppm and 2500-at.-ppm cases, the former for two distinct N^* . The width of $N_2(\nu, t)$ at short times exceeds the width of $g(\nu)$, obviously because of the dip in $p(\nu, t)$, but at longer times sinks under it, signifying the peaking up of $p(\nu, t)$. Already without conversion to $p(\nu, t)$, therefore, these data indicate a dramatic variation of the phonon spectrum with time. Of more interest in connection with spectral transport is, as the 700-at.-ppm data show, that the phonon spectrum remains flatter the higher N^* . This observation is, in fact, a direct indication that spectral transport takes place, and confirms previous results derived from the magnetic field dependence of the bottleneck at various N^* .⁷

Compelling evidence for spectral transport is derived from Fig. 7, in which the raw data, $R_2^{(obs)}(\nu, t)$, are plotted as a function of time for a selection of fixed distances $\Delta\nu$ from resonance. In fact, the four traces presented represent cross sections of a complete data set as in Fig. 2. The conditions pertaining to Fig. 7 are nearly identical to those for Fig. 2, except that, for improved statistics, fewer traces have been accumulated over longer times.

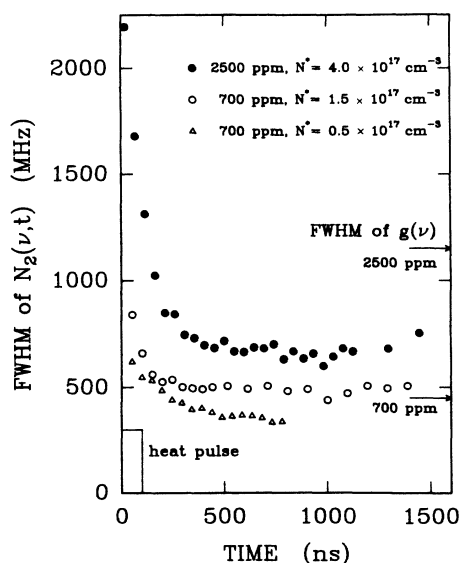


FIG. 6. Width of R_2 luminescence vs time after deconvolution for $I(\nu)$ and $\bar{R}_1(\nu)$ for 700-at.-ppm and 2500-at.-ppm ruby at the N^* indicated and $2R \approx 200 \mu\text{m}$. For comparison, the corresponding widths of the $\bar{E}(^2E)-2\bar{A}(^2E)$ line shape are also shown.

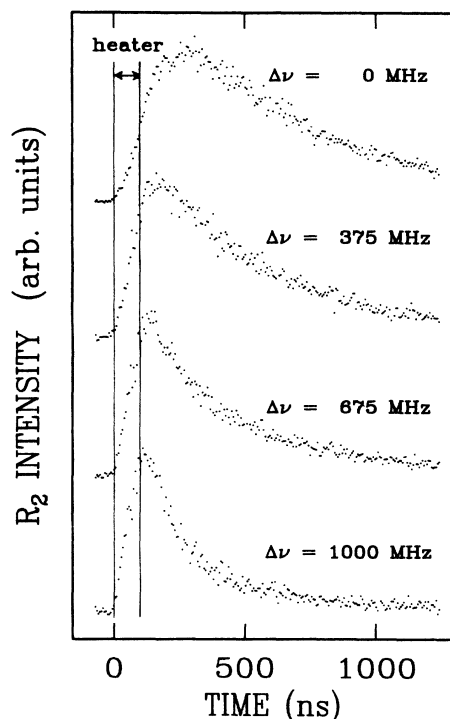


FIG. 7. Phonon-induced R_2 intensity vs time at fixed detection frequencies $\Delta\nu$ from the line center for 700-at.-ppm ruby at $N^* \approx 1.5 \times 10^{17} \text{ cm}^{-3}$ and $2R \approx 200 \mu\text{m}$. Intensities are in arbitrary units. The spread in the frequencies is 80 MHz.

Data collection at a limited number of frequencies does not, of course, permit deconvolution for $I(\nu)$ and $\bar{R}_1(\nu)$, so that the traces must, by necessity, be considered as averages over a range of frequencies extending over half the combined spread of $I(\nu)$ and $\bar{R}_1(\nu)$ to either side of the frequency settings, i.e., over the ranges 0 ± 80 , 375 ± 80 , 675 ± 80 , and 1000 ± 80 MHz. Figure 7 expresses quite directly the strong dependence of the phonon response on detuning. The most striking point is that near resonance $R_2(\nu, t)$, and thus $p(\nu, t)$, continues to rise after the heat pulse has been switched off. In the far wings, by contrast, $p(\nu, t)$ starts to decline immediately after the pulse. The external supply of phonons having ceased, there is no other conceivable source for the continued ingrowth of $p(\nu, t)$ near resonance than inelastic processes converting phonons in the wings to resonant ones. As we can see from the size of this afterfeeding in relation to the increase of $p(\nu, t)$ during the heat pulse, spectral transport, in fact, provides a substantial fraction of the feeding of near-resonant phonons. It should be pointed out with some emphasis that a release of externally supplied resonant phonons, which are trapped near the surface of the hot zone, cannot be held responsible for the continued ingrowth. These phonons stay in the hot zone no longer than, on the average, a time $\sigma^{1/2}\tau$, which, under the conditions of Fig. 7, amounts to 4 ns only. These findings have further been corroborated in a series of separate experiments, not discussed here, featuring

heat pulses of shorter duration and higher power.²⁷

In a detailed and realistic treatment of the way the temporal development of the phonon population is affected by spectral transport through the $\bar{E}(^2E)-2\bar{A}(^2E)$ transition, the phonon spectrum should, of course, be subdivided in mutually coupled packets sufficiently large in number to represent the line shape adequately. The associated set of coupled rate equations being untractable, we resort to Monte Carlo techniques to consider this explicitly (Sec. V B). A qualitative account may, however, be achieved by limiting ourselves for the moment to two generic classes of interacting phonons. Near-resonant phonons located within the initial depression of the phonon system are taken to form one class, while the other class is associated with off-resonant phonon modes that are efficiently fed by the heater. All phonons are assumed to be trapped by the spin system, i.e., the phonons are in dynamical equilibrium with the particular spin packet they are resonant with. As already pointed out, the spins, in effect, carry the larger part of the energy stored in the combined spin-phonon system [$N^*g(\nu) > \rho$]. The phonon populations pertaining to the two classes thus evolve according to the phenomenological rate equations

$$\begin{aligned} (N^*g + \rho)\Delta\nu \frac{dp}{dt} &= -\rho \Delta\nu \frac{p}{\tau} - \rho \Delta\nu \frac{p}{T_{st}} + \rho \Delta\nu' \frac{p'}{T_{st}}, \\ (N^*g' + \rho)\Delta\nu' \frac{dp'}{dt} &= -\rho \Delta\nu' \frac{p'}{\tau} - \rho \Delta\nu' \frac{p'}{T_{st}} \\ &\quad + \rho \Delta\nu \frac{p}{T_{st}} + \Phi, \end{aligned} \quad (6)$$

in which p denotes the occupation number averaged over the class of the near-resonant phonons, $\Delta\nu$ is the spectral

$$p(t)/p_\infty = \begin{cases} A[1 - \exp(-t/T_{\text{eff}}^*)] + (1-A)[1 - \exp(-t/T_{st}^*)], & t \leq t_p \\ A[1 - \exp(-t_p/T_{\text{eff}}^*)]\exp[-(t-t_p)/T_{\text{eff}}^*] + (1-A)[1 - \exp(-t_p/T_{st}^*)]\exp[-(t-t_p)/T_{st}^*], & t > t_p. \end{cases} \quad (9)$$

Here, the external phonon feeding is switched off at $t = t_p$, while $A = T_{\text{eff}}^*/(T_{\text{eff}}^* - T_{st}^*)$. Equation (9) has been fit to data sets like those in Fig. 7 for various settings of the detuning. For 700-at.-ppm ruby, the resultant T_{st}^* and T_{eff}^* are presented in Fig. 8 for three series of measurements, which differ only in the extent of the excited zone (diameter of the laser beam $\approx 50, 100,$ and $200 \mu\text{m}$). The excited-state concentration was held constant at $N^* \approx 1.5 \times 10^{17} \text{ cm}^{-3}$. These results demonstrate spectral transport from the data of Fig. 7 in yet another way. First, the development of the p 's is clearly nonexponential, indicating the presence of time constants besides T_{eff} . Second, the shorter time constant, to be associated with T_{st}^* , is peaked around resonance according to $g(\nu)$. This is indeed in conformity with Eq. (8) upon, by slightly heuristic arguments, converting g' to $g(\nu)$. The longer time constant T_{eff}^* , on the other hand, is flattened out with respect to $g(\nu)$, as is anticipated from Eq. (7). Note here that any reasonable frequency dependence of τ , having its maximum at resonance, would leave T_{eff}^* weakly

width of this class, g is the appropriate average of $g(\nu)$ near resonance, the quantities p' , $\Delta\nu'$, and g' similarly refer to the off-resonant modes, T_{st} is the time associated with spectral transport between the two classes, and Φ represents the feeding by the heat pulse. Note that the solutions of Eq. (6) return, as they should, to single-exponential decays with a time constant T_{eff} according to Eq. (4) in the event spectral transport is vanishingly small ($T_{st} \gg \tau$). Also note that the spectral transfer goes with the difference $p \Delta\nu - p' \Delta\nu'$, i.e., the net spectral transport scales with the gradient of the phonon occupation in the frequency domain.

In the framework of Eq. (6), the developments of p and p' with time are characterized by two time constants only. To lowest order in

$$(N^*g' + \rho)/(N^*g + \rho) \approx g'/g,$$

which is obviously smaller than unity, but for any value of T_{st} in relation to τ , these constant may be written

$$T_{\text{eff}}^* = \frac{1 + T_{st}/\tau}{2 + T_{st}/\tau} (N^*g/\rho + 1)\tau, \quad (7)$$

$$T_{st}^* = \frac{1}{1 + T_{st}/\tau} (N^*g'/\rho + 1)T_{st}. \quad (8)$$

For $T_{st} < \tau$, the time T_{eff}^* clearly is associated with the decay of the phonon population near resonance with the spin system, while T_{st}^* is the time scale on which the two classes of phonons achieve mutual equilibrium. Note the occurrence of g in the former, and g' in the latter time constant. The biexponential solution for p derived from Eq. (6) contains no parameters other than T_{eff}^* , T_{st}^* , and an overall prefactor p_∞ . The solution reads

dependent on the detuning. In measurements similar to those in Fig. 8, but not detailed here, similar observations have been found to hold for the 2500-at.-ppm. Verneuil-grown crystal at $N^* \approx 4 \times 10^{17} \text{ cm}^{-3}$ and $2R \approx 200 \mu\text{m}$.

In Fig. 9, we present the dependence of $T_{\text{eff}}^*(\Delta)$ and $T_{st}^*(\Delta)$ at the center of the resonance on the excited-state concentration N^* for both 700-at.-ppm and 2500-at.-ppm ruby. The data for $T_{\text{eff}}^*(\Delta)$ are distinct from the results for T_{eff} obtained in previous experiments^{1-4,28} in that T_{eff}^* pertains to a single phonon packet, rather than being the average of $T_{\text{eff}}^*(\nu)$ weighted according to $g(\nu)$ [cf. Eq. (1)]. Like $T_{\text{eff}}^*(\nu)$ averaged over the line, $T_{\text{eff}}^*(\Delta)$ increases more slowly with increasing N^* , but continues to rise. In an earlier publication,⁴ it was shown that the phonons suffer inelastic scattering by excited Cr^{3+} pairs, providing frequency displacements large enough for a trapped phonon to become a ballistic one (one-step wipeout). On this basis, the experimentally observed dependence of T_{eff} versus N^* was satisfactorily accounted for, in particular, the slow rise at the higher N^* . Further, it was found that

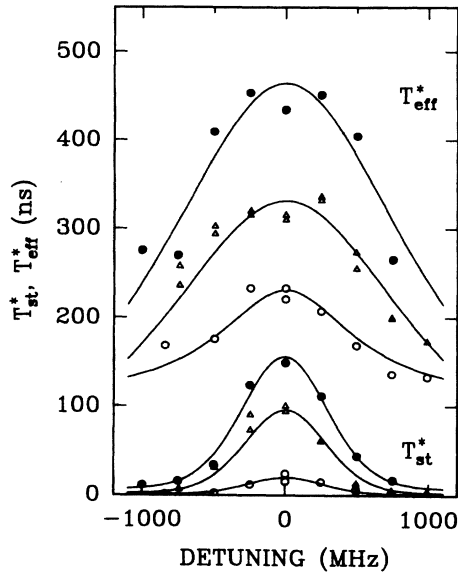


FIG. 8. T_{eff}^* and T_{st}^* vs frequency, obtained by fitting Eq. (9) to the data, for 700-at.-ppm ruby at $N^* \approx 1.5 \times 10^{17} \text{ cm}^{-3}$ and for various diameters of the pumped zone. $2R \approx 50, 100,$ and $200 \mu\text{m}$ (open circles, triangles, and solid circles, respectively).

the typical dimension of the excited zone, in the present case to be identified with the radius R , enters in quite a natural way upon comparison with the mean free path of the displaced phonon. Thus, the relevant combination of N^* and R occurring in T_{eff} appeared to be the product N^*R . In the present experiments a dependence of $T_{\text{eff}}^*(\Delta)$ on N^*R is, within errors, retrieved upon combin-

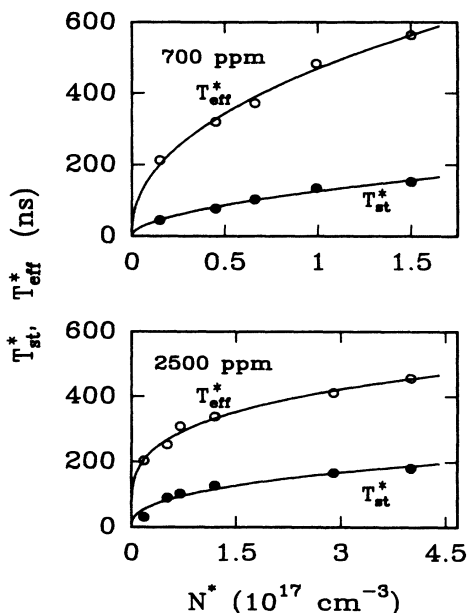


FIG. 9. T_{eff}^* and T_{st}^* vs N^* for 700-at.-ppm and 2500-at.-ppm ruby. In both cases $2R \approx 200 \mu\text{m}$.

ing Figs. 8 and 9. As concerns $T_{\text{st}}^*(\Delta)$, its N^* dependence resembles the N^* dependence of $T_{\text{eff}}^*(\Delta)$, while its R dependence seems to be somewhat stronger.

A note is in order on the determination of N^* , one of the most essential parameters in a quantitative treatment of phonon trapping. In the above experiments we excite, with a saturating laser beam, a homogeneous packet of Cr^{3+} out of one of the twofold degenerate 4A_2 ground states. The inhomogeneous width of the optical transition, $\Delta\nu_{\text{inh},R} \approx 3 \text{ GHz}$, is substantially smaller than the separation of 11.4 GHz between the two 4A_2 states. Under stationary excitation, therefore, N^* is not only determined by the ratio $\Delta\nu_{\text{hom},R}/\Delta\nu_{\text{inh},R}$, but further by the relaxation rate w ($\sim 10 \text{ s}^{-1}$) between the 4A_2 levels in relation to $1/\tau_R$. Unfortunately, w is not known to precision, inhibiting the determination of N^* . A time-resolved experiment in which saturation is reached well within a time $1/w$, however, allows us to relate the R_1 intensity to N^* .²⁹ In this case, of the ions in the 4A_2 component of departure, half of those on speaking terms with the laser are excited to $\bar{E}({}^2E)$. That is,

$$N_{\text{transient}}^* \approx \frac{1}{4} (\Delta\nu_{\text{hom},R} / \Delta\nu_{\text{inh},R}) N_0.$$

The N^* pertaining to stationary pumping is then found by scaling the result in proportion with the development of R_1 towards longer times. We thus find $N^* \approx 1.5 \times 10^{17} \text{ cm}^{-3}$ for the 700-at.-ppm crystal and $4 \times 10^{17} \text{ cm}^{-3}$ for the 2500-at.-ppm crystal under the conditions of the experiment. The values are estimated to be correct within half an order of magnitude. It is, however, noted that saturation and power broadening, increasing $\Delta\nu_{\text{hom},R}$, and microscopic strain broadening, reducing the local $\Delta\nu_{\text{inh},R}$, would both increase the estimated N^* .

V. DISCUSSION

The principal result of the experimental material presented in Sec. IV is the establishment of spectral transport within the phonon transition. A secondary finding is that direct external feeding of 29-cm⁻¹ phonons is ineffective near resonance. Spectral transport was found reflected in a flattening out of the phonon spectra with higher N^* , and, more directly, in afterfeeding of the central phonons once the external feeding has stopped. As is deduced from the weak frequency dependence of T_{eff}^* , spectral transport is quite efficient. On the other hand, spectral transport is not so effective as to completely dwarf the phonon processes associated with the phonon lifetime τ . This was seen in the decay traces at various detuning, which are not congruent, and in the depression in the phonon occupation as a result of the blocking out of direct resonant feeding, which persists under stationary conditions. Further, an important result is that T_{eff}^* and T_{st}^* have similar N^* dependences, indicating a common underlying mechanism.

A. Model

To account for the observed spectral dynamics of trapped 29-cm⁻¹ phonons, we rely on the model by Goossens *et al.*⁴ based on Cr³⁺ pairs coupled by weak exchange. The model has previously been successful in a quantitative interpretation of the N^* dependence of T_{eff} averaged over the phonon line shape.⁴ We consider a pair consisting of a metastable optically excited Cr³⁺ and a nearby Cr³⁺ in the 4A_2 ground state. The exchange interaction splits the double-degenerate $\bar{E}({}^2E)$ and $2\bar{A}({}^2E)$ states of the excited Cr³⁺ by the exchange parameter J . Because of the similarity of the spin parts of the $\bar{E}({}^2E)$ and $2\bar{A}({}^2E)$ states, however, the spin-nonflip separations of $\bar{E}({}^2E)$ and $2\bar{A}({}^2E)$ are to high degree insensitive to exchange. In other terms, the $\bar{E}({}^2E)$ - $2\bar{A}({}^2E)$ spin-nonflip transitions of the excited Cr³⁺ in the pair are at resonance with the spin-nonflip transitions of an excited Cr³⁺ in any other pair, or, for that matter, of any isolated metastable Cr³⁺. This situation provides spectral contact between phonons of distinct frequency by one-site resonant Raman processes, i.e., absorption of a phonon belonging to the central phonon packet in a spin-nonflip transition, and subsequent emission of a phonon shifted in frequency by $\pm J$ in a spin-flip transition. Within the model, two situations may be distinguished. If the frequency shift is large enough for the mean free path $\Lambda(\nu)$ to surpass the typical dimension of the excited zone (say, the radius R), the trapped phonon is converted into a ballistic one, which is lost by flight out of the hot zone. In the event the energy shift is so small that $\Lambda(\nu) < R$, however, the frequency-shifted phonon remains trapped in the excited zone, albeit less severely. Such a phonon may, in fact, be converted back into a phonon of the central packet by the reverse process. In Eqs. (6), the former case is to be identified with the τ process, and the latter case with the T_{st} processes. The model thus provides the common ground for T_{eff}^* and T_{st}^* inferred from the experiment. In dilute systems, the number of pairs obviously becomes larger with the Cr³⁺-Cr³⁺ distance. In the case of a truly random distribution of Cr³⁺ over the lattice and for an exchange interaction decaying with distance as

$$J = J_0 \exp(-ar), \quad (10)$$

the distribution of nearest-neighbor exchange parameters is given by⁴

$$D_J = \frac{4\pi N_0 [\ln(J/J_0)]^2}{a^3 J} \exp\left(\frac{4\pi N_0 [\ln(J/J_0)]^3}{3a^3}\right), \quad (11)$$

in which N_0 is the total concentration of Cr³⁺ ions. Theoretical estimates of the overlap integral have resulted in $a \approx 1 \text{ \AA}^{-1}$.^{30,31} By use of Eq. (10), optical absorption spectra of third- and fourth-nearest neighbors in the ground state then yield $J_0 \approx 330 \text{ cm}^{-1}$.³² Note that at a given N_0 the smaller J indeed carry most of the weight.

B. Monte Carlo simulations

For a more quantitative treatment of the spectral dynamics of 29-cm⁻¹ phonons in interaction with the excited Cr³⁺ ions, we have set up Monte Carlo simulations based upon the model just outlined, i.e., we follow the itinerary of externally generated phonons until escape at the boundary of the excited zone with explicit consideration of the modifications in their frequencies by Cr³⁺ pairs. We define, for simplicity, a simple cubic lattice of excited Cr³⁺ ions, such that N^* lattice points are contained in a unit of volume. The phonons are assumed to travel with a unique velocity from one lattice point to the next along nearest-neighbor connections, and their frequencies and directions of travel are permitted to change by interaction with the excited Cr³⁺. Aside from computational shortcuts, then, a Monte Carlo step runs as follows. When the phonon under consideration has reached an excited Cr³⁺, the latter is made part of an exchange-coupled pair by randomly drawing an exchange splitting J out of the D_J distribution. Next, the probabilities are calculated of all $\bar{E}({}^2E)_\pm \rightarrow 2\bar{A}({}^2E)_\pm \rightarrow \bar{E}({}^2E)_\pm$ processes, numbering eight in total, with due account of the widths of the relevant transitions. Here, the Zeeman levels $\bar{E}({}^2E)_\pm$ are assumed to be equally populated. A ninth "event" is the case of no interaction at all, its probability making up the probability missing from unity. One of these scattering events, randomly drawn with a weight according to its probability, is subsequently carried into effect. When an $\bar{E}({}^2E)_\pm \rightarrow 2\bar{A}({}^2E)_\pm \rightarrow \bar{E}({}^2E)_\pm$ process has been selected, the frequency of the phonon is, if necessary, appropriately modified, a new direction of travel is chosen out of the six allowed, and the age of the phonon is updated by adding to the time already incurred the time T_d the excitation on the average resides in $2\bar{A}({}^2E)$. In the event no interaction took place, the phonon is, of course, left to proceed on its course without modification and delay. The procedure is repeated upon encountering the next Cr³⁺ at a distance of a lattice constant until the phonon manages to escape the excited zone. Each time the phonon has undergone an $\bar{E}({}^2E)_\pm \rightarrow 2\bar{A}({}^2E)_\pm \rightarrow \bar{E}({}^2E)_\pm$ process, its frequency and age are registered in a frequency-time histogram. The histogram accordingly corresponds to the occupation $N_2(\nu, t)$ of $2\bar{A}({}^2E)$. The advantage of registering the $N_2(\nu, t)$ spectrum instead of the phonon spectrum is that the results are directly comparable with the experimental data. In turn, $p(\nu, t)$ may be derived from $N_2(\nu, t)$ by use of Eq. (1).

In the Monte Carlo simulations the response of the phonon population has been determined following injection of phonons from the heater at the instant $t=0$. The phonon spectrum, as it evolves with time in the case of a heat pulse of nonzero duration, is then derived by convoluting the response function obtained with the rectangular shape of the heat pulse. The duration of this pulse is, for sufficient statistics, taken to be 200 ns. In Fig. 10 we present the simulated phonon spectrum for a 700-at.-ppm ruby as it develops with time (the parameters adopted are discussed below). The main features of the experimental spectrum (Fig. 3), i.e., (i) the initial dip at resonance, and

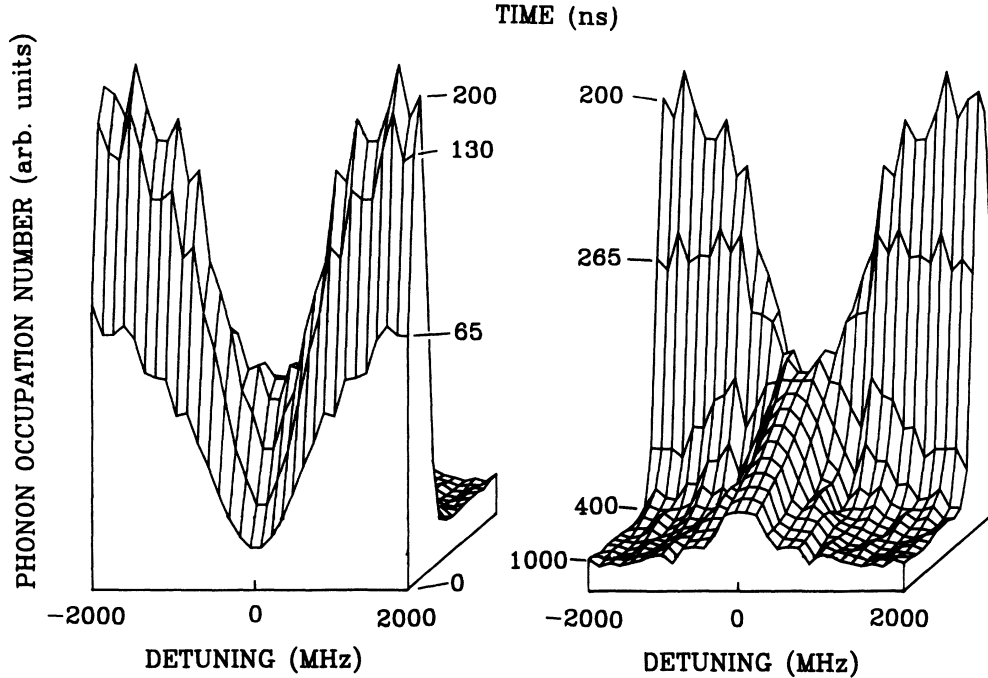


FIG. 10. Simulated phonon spectrum vs time for 700-at.-ppm ruby with $N^* = 6 \times 10^{17} \text{ cm}^{-3}$ in a volume of $0.2 \times 0.2 \times 10 \text{ mm}^3$. The pulse length is 200 ns. The life history of 10^4 phonons was followed. The resultant spectrum has been mirrored about zero detuning and the summed spectrum is shown. The plot shows only 1 in 32 calculated points.

(ii) the continued feeding of resonant phonons after the external feeding is switched off, both appear to be reproduced in the simulated spectrum. The afterfeeding of resonant phonons is most clearly demonstrated in Fig. 11, where we show the dependence of the spectrum on time at fixed phonon frequencies. The simulated dependences generally appear to resemble the experimental traces (Fig. 7). To facilitate a quantitative comparison with the latter, they have been parametrized by use of Eq. (9) based on the simplified approach of the two phonon classes. The results of the simulated T_{eff}^* and T_{st}^* are presented in Fig. 12.

Preparatory to a discussion of these results in comparison with experiment, it is expedient to specify a few details of the calculations and to examine the effects on T_{eff}^* and T_{st}^* of varying the parameters and the geometry entering the simulations. The spontaneous spin-flip and spin-nonflip times associated with $2\bar{A}(^2E)_{\pm} \rightarrow \bar{E}(^2E)_{\pm}$ were set at 1 and 12 ns, respectively, which are averages of literature values.³³ The phonon line shape $g(\nu)$ pertaining to single ions is a convolution of a significant inhomogeneous spread with the homogeneous lifetime broadening of $2\bar{A}(^2E)$. To improve computer efficiency, $g(\nu)$ has been made tractable as follows. Its homogeneous part has been represented by a normalized Lorentzian with a FWHM of $\Delta\nu_{\text{hom}} = 240 \text{ MHz}$.²⁰ As for the inhomogeneous spread, the spin-nonflip frequency of $\bar{E}(^2E) - 2\bar{A}(^2E)$ has been randomly drawn each time, simultaneously with the drawing of J , from a rectangular frequency distribution, centered around Δ and of such an extent that its convolution with the Lorentzian matches

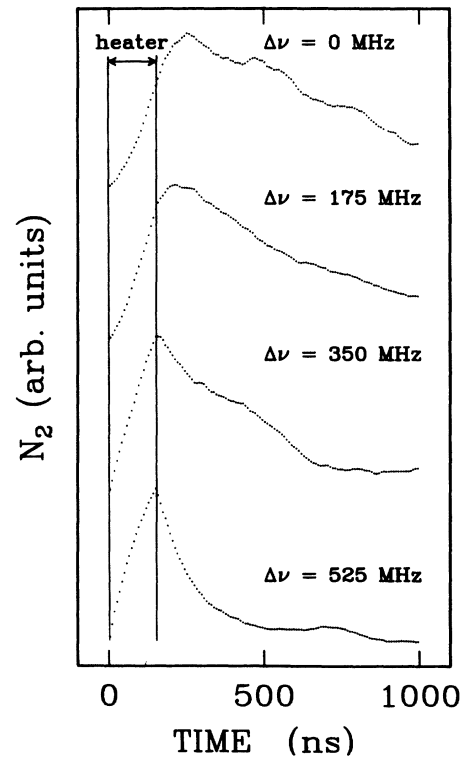


FIG. 11. Simulated occupation of $2\bar{A}(^2E)$, N_2 , vs time for 700-at.-ppm ruby at various distances $\Delta\nu$ from resonance. At a given $\Delta\nu$, the phonon occupation scales with N_2 . $N^* = 6 \times 10^{17} \text{ cm}^{-3}$ in a volume of $0.2 \times 0.2 \times 10 \text{ mm}^3$. The spectral resolution is 70 MHz.

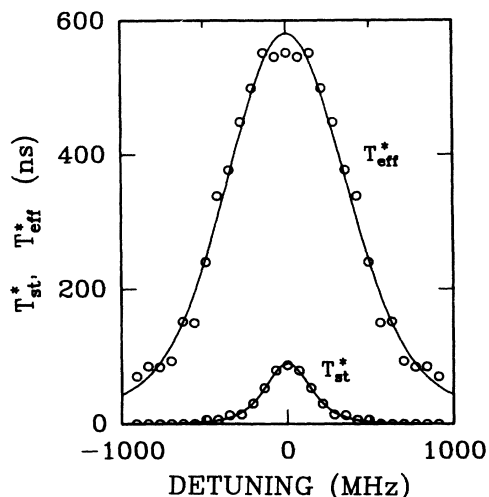


FIG. 12. Frequency dependences of T_{eff}^* and T_{st}^* derived from simulations at various detuning under conditions as in Figs. 10 and 11.

the experimental Voigt profile in width. The inhomogeneous interval appears to be 350-MHz wide for 700-at.-ppm ruby. It is known that the phonon linewidth of coupled pairs increases with the exchange.^{4,28} The additional broadening is not well understood, and may be of homogeneous, as well as inhomogeneous, nature. To incorporate this broadening, we have, in an admittedly heuristic way, let the width of the Lorentzian increase with an additional contribution amounting to γJ . The factor γ has been set to 0.6. Arguments for a γ of this magnitude are found in the dependence of T_{eff} on a magnetic field,⁴ and in recent calculations of the pair-state levels for various J .²⁸ While the zero-exchange line shape is adequately described, the exchange-induced broadening is, of course, subject to considerable uncertainty. A number of simulations have therefore been repeated for $\gamma=0$ and 2. For $\gamma=2$, the frequency dependence of T_{eff}^* and T_{st}^* do not turn out to be essentially altered in shape, but compared with the case $\gamma=0.6$ the time constants T_{eff}^* and T_{st}^* have increased by 15 and 25 %, respectively. For $\gamma=0$, T_{eff}^* has dropped by about a factor of 5. The case $\gamma=0$ is obviously not realistic. The drastic drop gives, however, expression to the effect of the exchange-induced broadening, which is to reduce the probability for wipeout of a central phonon.

Another quantity which is only known with limited precision is the exchange parameter of distant Cr^{3+} - Cr^{3+} pairs, i.e., the pairs responsible for spectral migration within the trapped phonon packet. In the calculations we used $a = 1.0 \text{ \AA}^{-1}$ and $J_0 = 330 \text{ cm}^{-1}$, in effect extrapolating, given a theoretical estimate for a , the J of pairs at the shorter distance of 3.5 \AA with the aid of Eq. (10). It is instructive, therefore, to consider the probability for a shift in the phonon frequency upon adopting other reasonable estimates of a , while maintaining the calibration of J at 3.5 \AA . In the example of Fig. 13, applying to an incoming phonon displaced from Δ by 600 MHz, the probability per encounter with a Cr^{3+} is given as a func-

tion of the frequency of the outgoing phonon for two combinations of a and J . Upon modifying the D_J distribution to $a = 0.7 \text{ \AA}^{-1}$ and $J_0 = 115 \text{ cm}^{-1}$, one observes a global enhancement of the inelastic scattering, obviously due to a corresponding increase in the number of scattering pairs in the range of J of relevance. In the simulations the increased transfer is borne out in a reduction of T_{st}^* by a factor of about 2.5. Remarkably, however, T_{eff}^* is not appreciably modified, in keeping with the notion that T_{eff}^* results from wipeout by the pairs with the larger J . A second point to note is that for a precisely resonant incoming phonon a graph such as Fig. 13 is symmetric about zero displacement, dropping according to D_J to either side. Ignoring elastic scattering, we thus see that phonons have a tendency to shift towards resonance, which is, of course, inherent to the model.

An important aspect in the geometry is that phonon production and phonon detection are disjunct in space. To replicate the experimental geometry of the hot zone as closely as possible, the grid has been permitted to extend over a volume of $0.2 \times 0.2 \times 10 \text{ mm}^3$. Phonons are incident at the center of one of the longer faces of this volume. The history of a phonon is followed until the phonon has left a detection zone of $0.2 \times 0.2 \times 1 \text{ mm}^3$, the longer dimension being commensurate with the size of the heater, but for, at most, $1 \mu\text{s}$. The phonon spectrum injected is assumed flat, spanning a range of 5 GHz to either side of the central frequency. The detection zone is taken to exclude the first $5 \mu\text{m}$ below the heater, where resonant phonons are trapped and for the majority

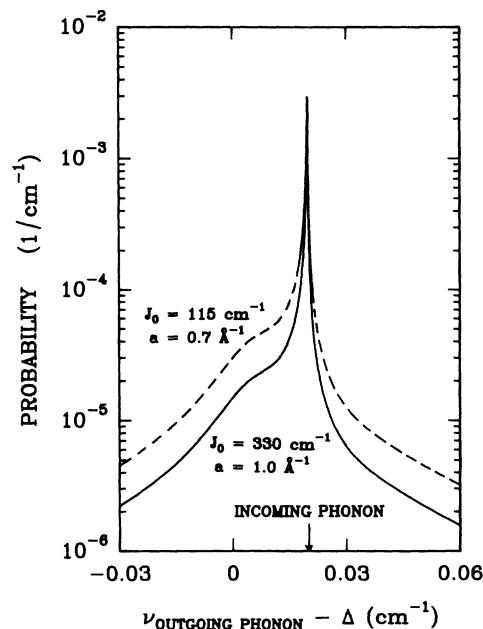


FIG. 13. Probability for a frequency shift of a phonon by interaction with a Cr^{3+} . The frequency of the incoming phonon is taken to be 600 MHz from Δ . $N_0 = 3.3 \times 10^{19} \text{ cm}^{-3}$, corresponding to 700-at.-ppm ruby. Two different sets of a and J_0 are considered. The set $a = 1.0 \text{ \AA}^{-1}$ and $J_0 = 330 \text{ cm}^{-1}$ is used in the simulations of Figs. 10–12.

reflected back into open space. Note again that at the relevant N^* (cf. Fig. 10) the mean free path Λ amounts to 1 μm only, increasing to 5 μm at twice the linewidth and to over 20 μm at 1000-MHz detuning. Indeed, if the detection zone is made to include the surface layer, an additional very fast spike (duration ≈ 10 ns) is registered on top of the traces of $N_2(\nu, t)$ versus time such as in Fig. 11. On the other hand, when the surface layer is made 25 μm deep, phonons penetrating the detection zone have dwindled in number to less than 10% of those initially injected. Of these, resonant phonons stem, as already noted, primarily from wipeout of nonresonant ones. Phonons penetrating at least 25 μm deep appear to exhibit the longer relaxation times characteristic of disappearance from the bulk, but remarkably the functional dependence of T_{eff}^* on the frequency has not appreciably changed. To examine the effects of the geometry further, we have performed simulations for a selection of other geometries, to find that the invariance of the functional dependence of T_{eff}^* on detuning is quite general, but that T_{eff}^* increases with the typical dimension of the hot zone. To give one example, when the zone is chosen as a cube of $0.2 \times 0.2 \times 0.2$ mm³, all T_{eff}^* become reduced by a factor of approximately 1.4 relative to the prolate geometry of Fig. 12, obviously because two more side faces become effective in escape.

We proceed with a comparison of the simulated decays (Fig. 11), or rather the frequency dependences of T_{eff}^* and T_{st}^* derived from these decays (Fig. 12), with the experimental results (Figs. 7 and 8). It is important to point out that this comparison subjects the frequency-shifting mechanism of the phonons to a very severe test, self-evidently much more severe than when the relaxation time is averaged over the phonon spectrum.^{3,4,28} In attempting to make the comparison quantitative, however, one is gravely hampered by the uncertainties in the parameters. We have just considered the effects of varying the quantity a , the exchange-induced broadening, and the geometry. Other parameters affecting the simulated T_{eff}^* and T_{st}^* obviously are $g(\nu)$ and N^* . All these effects are, to a large extent, correlated. To complicate matters further, the functional dependences taken for the exchange versus distance and the broadening may also differ from reality. The best approach, therefore, is to adhere to the reasonable choices for the parameters and functional dependences adopted above, and subsequently to judge whether the essential characteristics of the experimental results are duplicated. However, it is advantageous to vary N^* , the parameter which is the most uncertain, yet affects T_{eff}^* and T_{st}^* very directly. This we have, in fact, done in Figs. 11 and 12, adjusting N^* such that at the central phonon frequency $T_{\text{eff}}^*(\Delta)$ is somewhat overestimated, and $T_{\text{st}}^*(\Delta)$ somewhat underestimated in comparison with Fig. 8.

As it turns out, the overall resemblance is genuinely satisfactory. At their maxima, T_{eff}^* and T_{st}^* deviate from experiment by no more than 15 and 50%, respectively. The adjusted $N^* \approx 6 \times 10^{17}$ cm⁻³ appears to be four times the experimental value. It should be recalled, however, that the latter is already uncertain by about such a factor,

and likely is a lower limit (cf. last paragraph of Sec. IV), while the adjusted N^* in addition contains, as discussed above, uncertainties propagated from the other parameters. As concerns the frequency dependences of T_{st}^* and T_{eff}^* , T_{st}^* quite closely follows $g(\nu)$, as it does in the experiment. Also, the salient feature that T_{eff}^* drops considerably slower with frequency than, according to $g(\nu)$, is borne out by the simulations. Quantitatively, the FWHM of T_{st}^* versus frequency, which amounts to 350 MHz, compares favorably with the 440-MHz FWHM obtained from experiment, when due account is taken for the instrumental profile $I(\nu)$ and the spread $\tilde{R}_1(\nu)$, which together provide a broadening of about 200 MHz. At a detuning as large as 1000 MHz, the simulated T_{eff}^* has, however, dropped to about 80 ns, compared with roughly 200 ns from experiment. In reality, therefore, phonons displaced by a few times the linewidth appear to be imprisoned over longer periods than anticipated. The origin for this disparity is not understood in detail. So much is clear from the foregoing, however, modification of the parameters within acceptable limits does not result in substantial improvement. A minor improvement in $T_{\text{eff}}^*(\Delta)$ and $T_{\text{st}}^*(\Delta)$ is nonetheless achieved when raising a , and correspondingly J_0 , and at the same time lowering N^* or the size of the hot zone. These variations, however, do not significantly improve the frequency dependences.

As for possible explanations, it should be emphasized that mechanisms providing more efficient wipeout, such as resonant phonon-assisted energy transfer in the presence of microscopic broadening,³ would only make matters worse. From recent calculations of the pair states it was indeed inferred that at the relevant N^* resonant phonon-assisted energy transfer is infrequent.²⁸ The available experimental material, on the other hand, does not exclude that the energy-transfer process, which scales with the squared reciprocal energy mismatch, would be operative over very small shifts. Further, there are a number of alternatives as to why phonon relaxation is less effective in the wings. First, the pairs with the higher J , responsible for wipeout, are to some extent likely to be out of tune with the phonons. For the first few shells of neighbors, having J 's of over, say, 5 cm⁻¹, this is an established fact.⁶ Second, it is conceivable that D_J does not decrease with J as in Eq. (11), but drops faster at the higher J , which diminishes wipeout. Other modifications of D_J might derive from a distinction between the $M_J = \pm \frac{1}{2}$ and $\pm \frac{3}{2}$ states of the ground-state ion forming the pair.²⁸ A third mechanism could be a weak imprisonment of considerably detuned phonons by a "halo" of excitation surrounding the hot zone, and known to have a concentration of order 1% of N^* .²⁶ Finally, a possible mechanism is additional, nearly frequency-independent scattering by nonmetastable centers, such as Cr²⁺,³⁴ increasing elastic scattering, and thereby effectively elongating the ballistic flight time.

VI. CONCLUSIONS

A new method has made possible the direct observation of the spectra of trapped 29-cm⁻¹ phonons near res-

onance with the $\bar{E}(^2E)-2\bar{A}(^2E)$ transition in ruby. The method is based on the technique of FLN. Cr^{3+} are excited by narrow-band excitation to $\bar{E}(^2E)$, but unlike conventional FLN schemes, the phonon-induced luminescence of the nearby $2\bar{A}(^2E)$ level is used for high-resolution detection of nonequilibrium phonons. When followed as a function of time, the phonon spectra univocally point to substantial spectral redistribution within the nonequilibrium phonon distribution under severe trapping conditions. Although some of the early experiments concerning the phonon bottleneck gave evidence for spectral redistribution, it is only with the use of FLN that phonon detection has been proven possible with a spectral resolution better than the width of the trapped phonon packet. The effects of spectral transport manifested themselves in two different ways. First, because in our experiments in effect a nonuniform phonon spectrum is supplied, spectral transport is apparent in a flow of phonons towards resonance immediately after the external feeding has been switched off, and further in the associated non-single-exponential decay of the off-resonant phonons. Second, efficient spectral contact makes the relaxation of the combined phonon- $2\bar{A}(^2E)$ system more weakly dependent on the frequency than the intrinsic line shape of the transition.

The main features of the phonon dynamics observed in the experiments could be reproduced in a Monte Carlo

simulation following the random itinerary of a phonon until escape with explicit consideration of the various one-site elastic and inelastic scattering processes involving excited Cr^{3+} . The latter have their spin-flip transitions from $\bar{E}(^2E)$ to $2\bar{A}(^2E)$ modified by the exchange interaction with randomly positioned nearest-neighbor Cr^{3+} ions in the 4A_2 ground state. The simulation thus includes steps in frequency of all sizes, but with the weight on the small steps. As it appears, at the center of the transition, phonons take, on the average, many nearly elastic diffusive steps until a larger displacement in frequency results in wipeout. In the wings, however, a limited number of steps already leads to removal. It is finally noted that a useful extension of the present experiment would be to reduce the duration of the exciting pulse. This would emphasize excitation of phonons in the wings, where T_{eff}^* is smaller, and would permit the investigation of spectral transport over larger distances.

ACKNOWLEDGMENTS

The authors thank C. R. de Kok for invaluable technical assistance, and M. J. van den Boogaard for participation in the experiments. The work was supported by the Netherlands Foundation Fundamenteel Onderzoek der Materie (FOM) and the Nederlandse Organisatie voor Wetenschappelijk Onderzoek (NWO).

- ¹K. F. Renk and J. Deisenhofer, *Phys. Rev. Lett.* **26**, 764 (1971).
- ²J. I. Dijkhuis and H. W. de Wijn, *Solid State Commun.* **31**, 39 (1979); *Phys. Rev. B* **20**, 1844 (1979).
- ³R. S. Meltzer, J. E. Rives, and W. C. Egbert, *Phys. Rev. B* **25**, 3026 (1982).
- ⁴R. J. G. Goossens, J. I. Dijkhuis, and H. W. de Wijn, *Phys. Rev. B* **32**, 7065 (1985).
- ⁵S. A. Basun, A. A. Kaplyanskii, *Fiz. Tverd. Tela* **22**, 3500 (1980) [*Sov. Phys.—Solid State* **22**, 2055 (1980)]; A. A. Kaplyanskii, S. A. Basun, and V. L. Shekhtman, *J. Phys. (Paris)* **42**, C6-439 (1981).
- ⁶S. A. Basun, A. A. Kaplyanskii, S. P. Feofilov, and V. L. Shekhtman, *Fiz. Tverd. Tela* **25**, 2731 (1983) [*Sov. Phys.—Solid State* **25**, 1570 (1983)].
- ⁷J. I. Dijkhuis, A. van der Pol, and H. W. de Wijn, *Phys. Rev. Lett.* **37**, 1554 (1976).
- ⁸S. A. Basun, A. A. Kaplyanskii, and S. P. Feofilov, *Fiz. Tverd. Tela* **28**, 3116 (1986) [*Sov. Phys.—Solid State* **28**, 2038 (1986)].
- ⁹U. Happek, T. Holstein, and K. F. Renk, *Phys. Rev. Lett.* **54**, 2091 (1985).
- ¹⁰T. Holstein, S. K. Lyo, and R. Orbach, *Phys. Rev. Lett.* **36**, 891 (1976).
- ¹¹P. M. Selzer, D. S. Hamilton, and W. M. Yen, *Phys. Rev. Lett.* **38**, 858 (1977); P. M. Selzer and W. M. Yen, *Opt. Lett.* **1**, 90 (1977).
- ¹²P. E. Jessop and A. Szabo, *Phys. Rev. Lett.* **45**, 1712 (1980).
- ¹³S. Chu, H. M. Gibbs, S. L. McCall, and A. Passner, *Phys. Rev. Lett.* **45**, 1715 (1980).
- ¹⁴P. M. Selzer, D. L. Huber, B. B. Barnett, and W. M. Yen, *Phys. Rev. B* **17**, 4979 (1978).
- ¹⁵The magnetic field dependence of the 29-cm⁻¹ phonon dynamics is also accounted for by Monte Carlo simulations as set up in sec. V B [M. J. van Dort, M. J. van den Boogaard, J. I. Dijkhuis, and H. W. de Wijn (unpublished)]. However, the magnetic field dependence measured in Ref. 4 appears to be at variance with the dependence reported in Ref. 28, which points to an appreciable phonon-assisted energy transfer.
- ¹⁶A. Szabo, *Phys. Rev. B* **25**, 924 (1970).
- ¹⁷W. M. Yen and P. M. Selzer, in *Laser Spectroscopy in Solids*, Vol. 49 of *Topics in Applied Physics*, edited by W. M. Yen and P. M. Selzer (Springer-Verlag, Berlin, 1981), p. 141.
- ¹⁸P. E. Jessop, T. Muramoto, and A. Szabo, *Phys. Rev. B* **21**, 926 (1980). The number quoted applies to 200-at.-ppm ruby. FLN work by us on a 700-at.-ppm sample yielded $\Delta\nu_{\text{hom},R} = 74 \pm 8$ MHz.
- ¹⁹N. Retzer, H. Lengfellner, and K. F. Renk, *Phys. Lett.* **96A**, 487 (1983).
- ²⁰M. J. van Dort, M. H. F. Overwijk, J. I. Dijkhuis, and H. W. de Wijn, *Solid State Commun.* **72**, 237 (1989).
- ²¹R. J. von Gutfeld and A. H. Nethercot, *Phys. Rev. Lett.* **12**, 641 (1964).
- ²²W. E. Bron, *Rep. Prog. Phys.* **43**, 301 (1980).
- ²³In a preliminary analysis of $R_2(\nu, t)$ [M. J. van Dort, J. I. Dijkhuis, and H. W. de Wijn, *J. Lumin.* **38**, 217 (1987)], $g(\nu)$ was approximated by a Lorentzian. The Lorentzian overshoots $g(\nu)$ in the wings, thereby underestimating $p(\nu, t)$.
- ²⁴M. H. F. Overwijk, J. I. Dijkhuis, and H. W. de Wijn (unpublished).
- ²⁵The absolute calibration of $p(\nu, t)$ contains, of course, an addi-

- tional uncertainty related to the ratio of the transition probabilities of the *R* lines and possible reabsorption of the luminescences.
- ²⁶R. J. G. Goossens, J. I. Dijkhuis, and H. W. de Wijn, *J. Lumin.* **34**, 19 (1985).
- ²⁷K. Z. Troost, J. I. Dijkhuis, and H. W. de Wijn (unpublished).
- ²⁸S. Majetich, R. S. Meltzer, and J. E. Rives, *Phys. Rev. B* **38**, 11 075 (1988).
- ²⁹A. Szabo, *Phys. Rev. B* **11**, 4512 (1975).
- ³⁰S. K. Lyo, *Phys. Rev. B* **3**, 3331 (1971).
- ³¹Nai Li Huang, R. Orbach, E. Šimánek, J. Owen, and D. R. Taylor, *Phys. Rev.* **156**, 383 (1967).
- ³²P. Kisliuk, N. C. Chang, P. L. Scott, and M. H. L. Pryce, *Phys. Rev.* **184**, 367 (1969).
- ³³J. E. Rives and R. S. Meltzer, *Phys. Rev. B* **16**, 1808 (1977); N. Retzer, H. Lengfellner, and K. F. Renk, *Phys. Lett.* **96A**, 487 (1983); see also Ref. 20.
- ³⁴K. F. Renk, in *Phonon Scattering in Condensed Matter*, edited by W. Eisenmenger, K. Lassmann, and S. Döttinger (Springer-Verlag, Berlin, 1984), p. 10.